Ultrafast Structure Switching through Nonlinear Phononics

D. M. Juraschek,* M. Fechner, and N. A. Spaldin
Materials Theory, ETH Zurich, CH-8093 Zürich, Switzerland
(Received 21 July 2016; published 31 January 2017)

We describe a mechanism by which nonlinear phononics allows ultrafast coherent and directional control of transient structural distortions. With $ErFeO_3$ as a model system, we use density functional theory to calculate the structural properties as input into an anharmonic phonon model that describes the response of the system to a pulsed optical excitation. We find that the trilinear coupling of two orthogonal infrared-active phonons to a Raman-active phonon causes a transient distortion of the lattice. In contrast to the quadratic-linear coupling that has been previously explored, the direction of the distortion is determined by the polarization of the exciting light, introducing a novel mechanism for nonlinear phononic switching. Since the occurrence of the coupling is determined by the symmetry of the system we propose that it is a universal feature of orthorhombic and tetragonal perovskites.

DOI: 10.1103/PhysRevLett.118.054101

Over the last decade it has been shown repeatedly that laser excitation of infrared-active phonons is a powerful tool for modifying the properties of materials. This *dynamical materials design* approach has been used to drive metal-insulator transitions [1,2], to melt orbital order [3,4] and to induce superconductivity or modify superconducting transition temperatures [5,6] in a range of complex oxides. Particularly intriguing is the case in which the laser intensity is so high that the usual harmonic approximation for the lattice dynamics breaks down and anharmonic phonon-phonon interactions become important. Recent experimental and theoretical studies [7,8] have clarified that quadratic-linear cubic coupling of the form $Q_{\mathrm{IR}}^2 Q_{\mathrm{R}}$ between a driven infrared-active mode, Q_{IR}, and a Raman-active mode, Q_{R}, causes a shift in the equilibrium structure to a nonzero value of the Raman mode normal coordinates. This nonlinear phononic effect has most notably been associated with the observation of coherent transport, an indicator of superconductivity, far above the usual superconducting Curie temperature in underdoped $YBaCu_3O_{6+\delta}$ [9–11].

Here we demonstrate that cubic phononic coupling of the trilinear form $Q_{\mathrm{IR}_1} Q_{\mathrm{IR}_2} Q_{\mathrm{R}}$, in which two different infrared-active (IR) modes are excited simultaneously and couple anharmonically to a single Raman mode, provides an additional, even more appealing, pathway for dynamical control of materials. In addition to the change in equilibrium structure already demonstrated using quadratic-linear coupling, we show that such trilinear coupling enables control of the *direction* of the transient distortion. This provides a mechanism for nonlinear phononic switching of structural distortions that is straightforwardly achieved experimentally by changing the polarization of the incident light pulse [12].

Our motivation is provided by recent experimental work on the perovskite-structure orthoferrite $ErFeO_3$ [13], in which two polar modes of similar frequencies with atomic displacement patterns along the inequivalent *a* and *b* orthorhombic axes were simultaneously excited. Reference [13] reported and analyzed the resulting excitation of a magnon; here our focus is on the changes caused by and the implications of the nonlinear phonon dynamics.

$ErFeO_3$ is a distorted perovskite with the orthorhombic *Pbnm* structure and the typical *G*-type antiferromagnetic ordering of the Fe^{3+} magnetic moments [14] (Fig. 1). The primitive magnetic unit cell contains 20 atoms, resulting in 60 phonon modes characterized by representations (within the orthorhombic point group *mmm*) A_g, $B_{(1,2,3)g}$, A_u, and $B_{(1,2,3)u}$. Of the polar "*u*" modes, only B_{1u}, B_{2u}, and B_{3u} have dipole moments and are therefore excitable by midinfrared light. Since $ErFeO_3$ is centrosymmetric, there is no nonlinear second-harmonic optical response to the laser excitation.

The totally symmetric representation in the *mmm* point group is A_g, and so coupling is only symmetry allowed between combinations of phonon modes whose product contains the A_g representation. To cubic order, and for excitation of the B_u modes, this is the case for two types of mode combinations: quadratic-linear $B_{iu}^2 A_{\mathrm{g}}$ and trilinear

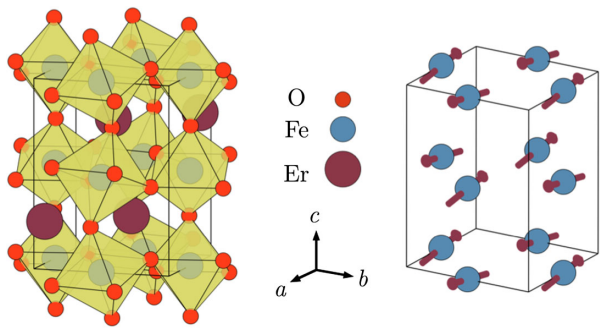

FIG. 1. *Pbnm* lattice structure of $ErFeO_3$. The left unit cell shows the tilted octahedra of the distorted perovskite structure. The right unit cell shows the *G*-type antiferromagnetic ordering of the iron spins along the *a* axis.

$B_{iu}B_{ju}B_{kg}$, where $\{i,j,k\} = \{1,2,3\}, i \neq j \neq k$. The quadratic-linear case describes the coupling of a single optically excited polar mode to a symmetric A_g Raman mode, and is the nonlinear phononic scenario that has been studied previously [8–11,15,16]. In this work we focus instead on the trilinear case in which two IR modes with different symmetries are excited and combine with a B_{kg} mode. We note also that in quartic order, any combination of infrared and Raman modes of the biquadratic form $Q_{\mathrm{IR}}^2 Q_{\mathrm{R}}^2$ results in an A_g representation, and so the potential energy up to fourth order can be written as

$$\begin{aligned} V(\mathbf{Q}) = {} & \frac{\omega_1^2}{2} Q_{\mathrm{IR}_1}^2 + \frac{\omega_2^2}{2} Q_{\mathrm{IR}_2}^2 + \frac{\omega_{\mathrm{R}}^2}{2} Q_{\mathrm{R}}^2 \\ & + c_{\mathrm{R}} Q_{\mathrm{R}}^3 + c_{1\mathrm{R}} Q_{\mathrm{IR}_1}^2 Q_{\mathrm{R}} + c_{2\mathrm{R}} Q_{\mathrm{IR}_2}^2 Q_{\mathrm{R}} \\ & + c_{12\mathrm{R}} Q_{\mathrm{IR}_1} Q_{\mathrm{IR}_2} Q_{\mathrm{R}} + \frac{d_1}{4} Q_{\mathrm{IR}_1}^4 + \frac{d_2}{4} Q_{\mathrm{IR}_2}^4 + \frac{d_{\mathrm{R}}}{4} Q_{\mathrm{R}}^4 \\ & + d_{12} Q_{\mathrm{IR}_1}^2 Q_{\mathrm{IR}_2}^2 + d_{1\mathrm{R}} Q_{\mathrm{IR}_1}^2 Q_{\mathrm{R}}^2 + d_{2\mathrm{R}} Q_{\mathrm{IR}_2}^2 Q_{\mathrm{R}}^2, \quad (1) \end{aligned}$$

where Q_{IR_1} and Q_{IR_2} denote the amplitudes of IR modes with different symmetries and eigenfrequencies ω_1 and ω_2 and Q_{R} is the amplitude of a Raman mode with eigenfrequency ω_{R}. The coefficients $\{c\}$ and $\{d\}$ define the strengths of the cubic and quartic anharmonicity and are material specific. As stated above, $c_{\mathrm{R}} = c_{1\mathrm{R}} = c_{2\mathrm{R}} = 0$ by symmetry if Q_{R} corresponds to a B_{ig} mode and $c_{12\mathrm{R}} = 0$ if Q_{R} corresponds to an A_g mode.

We will see that the quartic coefficients in $ErFeO_3$ are small, consistent with earlier work for related transition metal oxides [11], and since we are interested in isolating the effects of the trilinear coupling, we analyze the reduced potential

$$\begin{aligned} V(\mathbf{Q}) = {} & \frac{\omega_1^2}{2} Q_{\mathrm{IR}_1}^2 + \frac{\omega_2^2}{2} Q_{\mathrm{IR}_2}^2 + \frac{\omega_{\mathrm{R}}^2}{2} Q_{\mathrm{R}}^2 \\ & + c_{12\mathrm{R}} Q_{\mathrm{IR}_1} Q_{\mathrm{IR}_2} Q_{\mathrm{R}} \quad (2) \end{aligned}$$

in the following. The value of Q_{R} that minimizes $V(\mathbf{Q})$, and which corresponds to the average structure induced by the trilinear coupling, is obtained trivially from this expression as

$$Q_{\mathrm{R}_{\mathrm{min}}} = \frac{c_{12\mathrm{R}} Q_{\mathrm{IR}_1} Q_{\mathrm{IR}_2}}{\omega_{\mathrm{R}}^2}. \quad (3)$$

We therefore expect that the induced structural distortions will be largest for low-frequency Raman modes with large $c_{12\mathrm{R}}$ coupling coefficients.

We begin by calculating the structural properties of $ErFeO_3$ from first principles within the density functional formalism as implemented in the Vienna *ab initio* simulation package (VASP) [17,18]. We used the default VASP PAW pseudopotentials with valence electronic configurations Er ($6s^2 5p^6 5d^1$), Fe ($3d^7 4s^1$) and O ($2s^2 2p^4$), with the $4f$ electrons of erbium in the core. Treatment of the $4f$ electrons as core states has the desirable side effect of yielding the room-temperature magnetic structure, with the iron spins oriented along the a axis and a weak ferromagnetic moment along c [14] (Fig. 1), in our zero kelvin calculation, since the experimentally observed low-temperature spin-reorientation transitions to other easy axes [19], attributed to interaction with the Er $4f$ moments, are suppressed. Good convergence was obtained with a plane-wave energy cut-off of 850 eV and a $6 \times 6 \times 4$ k-point mesh to sample the Brillouin zone. We converged the Hellmann-Feynman forces to 10^{-5} eV/Å for the calculation of phonons with the frozen-phonon method as implemented in the phonopy package [20]. For the exchange-correlation functional we chose the PBEsol [21] form of the generalized gradient approximation (GGA) with a Hubbard U correction on the Fe $3d$ states. We found that an on-site Coulomb interaction of $U = 3.7$ eV and a Hund's exchange of $J = 0.7$ eV optimally reproduce both the lattice dynamical properties [13,22,23] and the G-type antiferromagnetic ordering [14] as well as the photoemission spectrum of closely related $LaFeO_3$ [24]. In particular we found that phonon eigenfrequencies are underestimated by other approaches, including the usual PBE functionals. Our fully relaxed structure with lattice constants $a = 5.19$ Å, $b = 5.56$ Å, and $c = 7.52$ Å fits reasonably well to the experimental values of Ref. [25], as do our calculated phonon eigenfrequencies. Anharmonic coupling constants were computed by calculating the total energies as a function of ion displacements along the normal mode coordinates of every Q_{R} mode and of every Q_{IR_1} and Q_{IR_2} mode that it couples to and then fitting the resulting three-dimensional energy landscape to the potential V of Eq. (1).

In the experiment of Ref. [13], the laser pulse was directed perpendicular to the short axes a and b of the orthorhombic $ErFeO_3$ crystal. The phonons that are excited by such a pulse have symmetries B_{3u} (polarization along the a axis) and B_{2u} (polarization along the b axis). The trilinear coupling term is therefore only nonzero for Raman modes of B_{1g} symmetry; both IR modes couple quadratic linearly to A_g Raman modes. The experimental 130 fs pulse had a mean frequency of $\omega_0 = 19.5$ THz with a full width at half maximum of 3.4 THz, so that IR modes between around 15 and 20 THz are significantly excited by the pulse. Our calculated values for the phonon eigenfrequencies with symmetries B_{3u}, B_{2u}, A_g, and B_{1g} are listed in Table I (for the full list of calculated eigenfrequencies see the Supplemental Material [26]) along with available experimental values. In Fig. 2(a) we show a model midinfrared laser pulse with the properties of that used in Ref. [13] and indicate our calculated B_{3u} and B_{2u} eigenfrequencies with vertical lines. We see that phonon modes with B_{3u} and B_{2u} symmetries occur in pairs of similar eigenfrequencies, consistent with the small orthorhombicity of $ErFeO_3$ (in a tetragonal structure they would form a pair of degenerate E_u modes). It is also clear from

TABLE I. Calculated and experimental phonon eigenfrequencies in THz. Infrared data were taken from Refs. [13,22], Raman data from Ref. [23].

Symmetry	DFT	Experiment	Symmetry	DFT	Experiment
A_g	3.3	3.4	B_{1g}	3.2	3.4
	4.0	4.0		4.8	4.8
	8.1	8.1		9.6	9.7
	10.0	10.0		10.5	⋯
	12.5	12.4		14.6	15.1
	13.0	13.0		16.2	⋯
	14.9	14.9		18.3	⋯
B_{2u}	3.1	⋯	B_{3u}	3.5	⋯
	5.7	⋯		5.2	⋯
	7.2	⋯		7.5	⋯
	8.9	⋯		8.6	⋯
	9.7	⋯		9.9	⋯
	10.2	⋯		10.9	10.9
	13.2	13.3		12.4	⋯
	15.7	⋯		15.5	⋯
	16.0	16.2		16.5	17.0

Fig. 2(a) that only the group of four IR modes with the highest eigenfrequencies $B_{3u}(16.5)$, $B_{2u}(16.0)$, $B_{2u}(15.7)$, and $B_{3u}(15.5)$ are significantly excited by the pulse of Ref. [13]. We show the displacements of the oxygen ions in the eigenvectors of these modes, and the direction of the corresponding polarization in Figs. 2(b)–2(e). In the following analysis we focus on the two highest frequency modes, $B_{3u}(16.5)$ and $B_{2u}(16.0)$ and the lowest frequency Raman modes, $B_{1g}(3.2)$ and $A_g(3.3)$, for which we expect the biggest effect according to Eq. (3).

Our calculated values for the anharmonic coefficients $\{c\}$ and $\{d\}$ for these modes are shown in Table II with the list of coefficients for the remaining combinations of the four highest frequency IR modes given in the Supplemental Material [26]. We see that the quartic order coupling coefficients between Raman and IR modes, d_{1R} and d_{2R}, are all at least 1 order of magnitude smaller than the cubic coupling coefficients, c_{1R}, c_{2R}, and c_{12R}. (Note that the other anharmonic coefficients listed for completeness do not couple Raman and IR modes). This confirms our expectation that phonon-phonon coupling of the biquadratic kind is negligible for the dynamics of this system. We see also that the coefficient of trilinear coupling to the B_{1g} mode is similar in magnitude (in fact slightly larger) to that of the quadratic-linear coupling to the A_g mode.

To investigate the evolution of the anharmonic system, we next solve numerically the dynamical equations of motion that form the system of coupled differential equations:

$$\ddot{\mathbf{Q}} + \gamma\dot{\mathbf{Q}} + \nabla_{\mathbf{Q}}[V(\mathbf{Q}) - F(t,\theta)Q_{\mathrm{IR}}] = 0, \qquad (4)$$

where $\mathbf{Q} = (Q_{\mathrm{IR}_1}, Q_{\mathrm{IR}_2}, Q_{\mathrm{R}})$ describes both the excited IR modes and one Raman mode that couples to them. γ is the linewidth (inverse lifetime) of each mode and $F(t,\theta)$ the

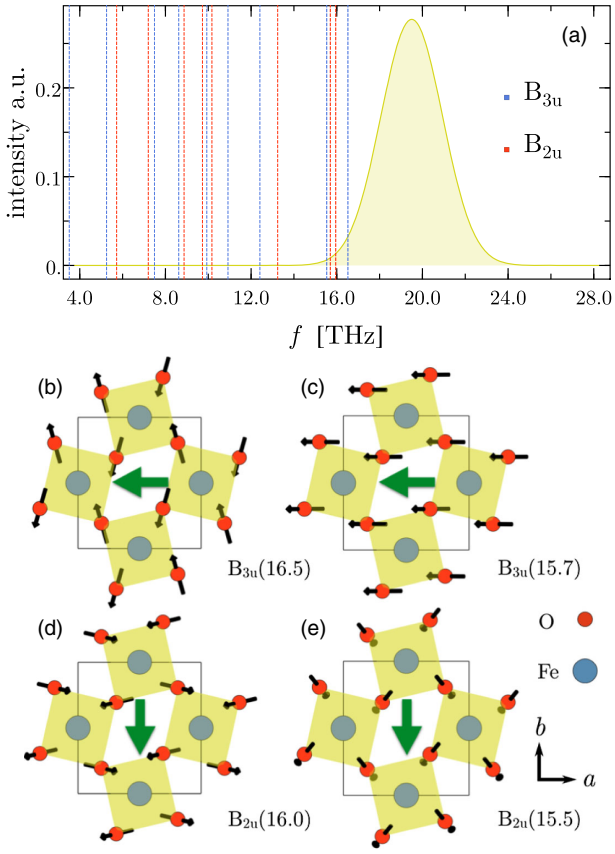

FIG. 2. (a) Frequency spectrum of a 130 fs model pump pulse with mean frequency $\omega_0 = 19.5$ THz and a full width at half maximum of 3.4 THz as used in Ref. [13]. Our calculated phonon eigenfrequencies for $ErFeO_3$ are shown as vertical dashed lines, with the four highest frequency modes that we consider in this work marked as thicker dashed lines. The right panels show the displacements of the oxygen ions in modes (b) $B_{3u}(16.5)$, (c) $B_{2u}(16.0)$, (d) $B_{2u}(15.7)$, and (e) $B_{3u}(15.5)$ as thin black arrows and the resulting direction of polarization as thick green arrows.

driving force on the IR modes that represents the laser pulse (for the exact form of F see the Supplemental Material [26]). θ is the polarization angle of the linearly polarized light from the laser with $\theta = 0°$ corresponding to a polarization along the a axis of the crystal and $\theta = 90°$ to a polarization along the b axis. The evolution of the system after an excitation

TABLE II. Anharmonic coefficients for the two Raman modes with lowest eigenfrequencies that couple to the $B_{3u}(16.5)$ and $B_{2u}(16.0)$ IR modes. Units are $\mathrm{meV}/(\text{Å}\sqrt{\mu})^n$, where μ is the atomic mass unit and n the order of the phonon amplitude. The $\{c\}$ coefficients with 0 value vanish due to symmetry arguments, whereas d_{1R} for the B_{1g} mode is accidentally zero.

	c_R	c_{1R}	c_{2R}	c_{12R}	d_1	d_2	d_R	d_{12}	d_{1R}	d_{2R}
$B_{1g}(3.2)$	0	0	0	−10.2	17.6	8.2	1.1	12.0	0.0	−0.1
A_g (3.3)	−0.5	7.8	3.7	0	17.6	8.2	1.1	12.0	−0.3	0.1

with the laser pulse is shown in Figs. 3(a)–3(d) for different polarization angles. The displacements of the oxygen ions corresponding to the $B_{1g}(3.2)$ and $A_g(3.3)$ Raman modes are shown in Figs. 3(e) and 3(f).

In Figs. 3(a) and 3(b) the polarization of the light pulse is along one of the lattice vectors so that in each case only IR modes of one symmetry type are excited, B_{3u} in Fig. 3(a), where the pulse is oriented along the a axis ($\theta = 0°$) and B_{2u} in Fig. 3(b), for a pulse along the b axis ($\theta = 90°$). As a result there is no trilinear coupling and no excitation of the $B_{1g}(3.2)$ mode. In both cases, the $A_g(3.3)$ mode is excited through its quadratic-linear coupling to the single IR mode. We see that its sinusoidal oscillation (blue line) is not centered around zero amplitude indicating the characteristic transient structural distortion caused by the quadratic-linear coupling $Q_{\mathrm{IR}}^2 Q_{\mathrm{R}}$, as observed previously in Refs. [9–11,15,16] and described above. The induced shifts of the minimum in the potential for the Raman mode are shown in the insets. Since the potential depends quadratically on the IR mode, and the signs of the coupling coefficients $c_{1\mathrm{R}}$ and $c_{2\mathrm{R}}$ are the same, the direction of the structural distortion is independent of the angle of its polarization, with the same direction of shift for $\theta = 0°$ and $\theta = 90°$. Note, however, that the strength of the quadratic-linear coupling as different in the two cases, since the values of the coupling coefficients $c_{1\mathrm{R}}$ and $c_{2\mathrm{R}}$ differ.

In Figs. 3(c) and 3(d) the polarization of the light pulse is midway between the lattice vectors, at $\theta = +45°$ and $\theta = -45°$, respectively, so that both IR modes are excited simultaneously. In this case the response of the B_{1g} mode is maximal. The behavior of the A_g mode is the same as the previous cases, with the amplitude and direction of the shift in the average value independent of the polarization of the pulse. The trilinear coupling $Q_{\mathrm{IR}_1} Q_{\mathrm{IR}_2} Q_{\mathrm{R}}$ of the $B_{1g}(3.2)$ mode shows strikingly a different behavior, however. We see that when the polarization angle is changed from $\theta = +45°$ to $\theta = -45°$, the trilinear coupling term changes sign, and the transient deformation of the lattice is in the opposite direction along the normal mode coordinates of the B_{1g} mode.

The time for which the transient structural deformation of the B_{1g} mode maintains its initial direction is determined by the inverse difference frequency $|\omega_1 - \omega_2|^{-1}$, which determines the time scale of the dephasing. The smaller the difference frequency of the IR modes, the longer it takes them to dephase and thus the longer the directional selectivity of the trilinear coupling persists. For the realistic linewidth that we assumed, the structural shift relaxes back to the ground state over the time scale of approximately one picosecond. Over this interval the IR modes to not dephase noticeably. In the case of a tetragonal structure in which the in-plane IR modes form a degenerate E_u pair, $\omega_1 = \omega_2$ and no dephasing occurs. In this limit both quadratic-linear *and* trilinear coupling to a fully symmetric A_{1g} Raman mode should occur simultaneously, with their relative strengths determined by the angle of the excitation pulse to the crystallographic axes.

In summary, we have shown that excitation of two infrared-active (IR) phonon modes with different

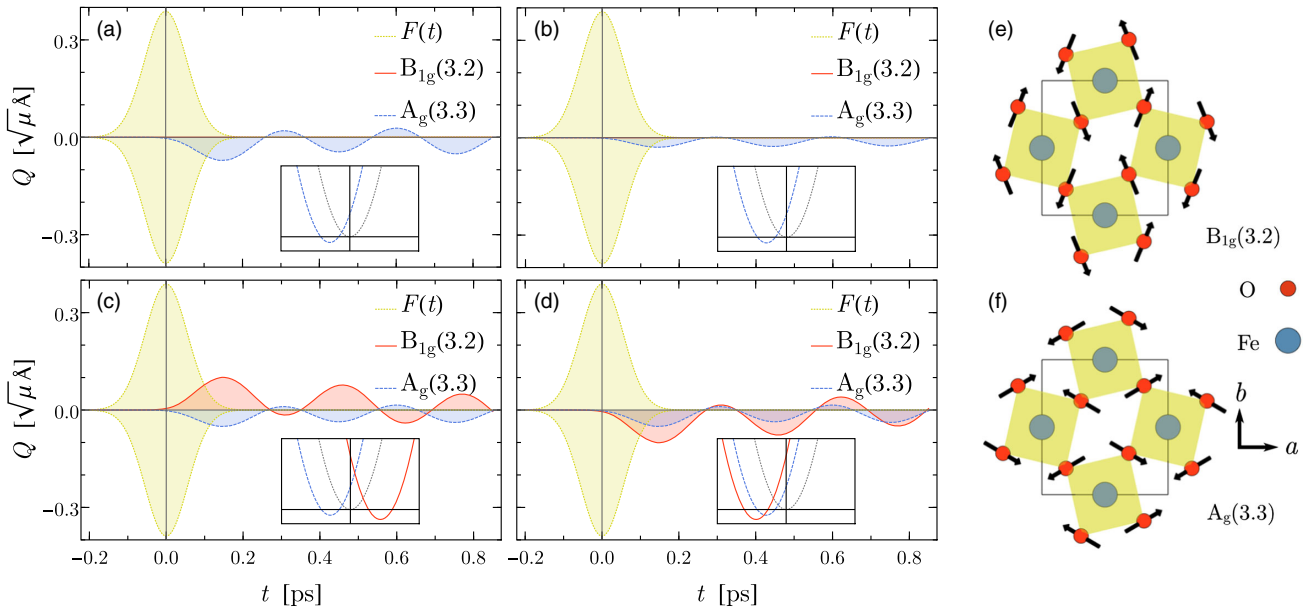

FIG. 3. Evolution of the two Raman modes with lowest eigenfrequencies when pumped with linearly polarized light at (a) $\theta = 0°$, (b) $\theta = 90°$, (c) $\theta = +45°$, and (d) $\theta = -45°$, with $\theta = 0°$ corresponding to a polarization along the a axis of the crystal and $\theta = 90°$ to a polarization along the b axis. We assumed a realistic linewidth of $\gamma \approx f/20$ [13]. The shifts in the minima of the Raman modes are shown schematically in the insets, with the gray curve indicating an unshifted potential, and blue and red the shifted A_g and B_{1g} potential, respectively. The right panel shows the displacements of the oxygen ions corresponding to the modes (e) $B_{1g}(3.2)$ and (f) $A_g(3.3)$.

symmetries but similar eigenfrequencies in the orthorhombic perovskite $ErFeO_3$ causes a transient structural distortion along the eigenvectors of a coupled B_{1g} Raman mode as a result of its trilinear coupling with the IR modes. In contrast to the quadratic-linear coupling of a symmetric A_g Raman mode to a *single* IR mode that has been discussed previously [8–11,15,16] and which we also observe here, the direction of the transient distortion is determined by the polarization of the excitation pulse relative to the crystallographic axes and can be reversed by reversing the polarization direction. While the analysis presented here was performed for $ErFeO_3$, it is directly applicable to all orthorhombic and tetragonal perovskites, with the strengths of the coupling constants and the values of the phonon frequencies of course being material dependent; extension to other crystal classes involves a further straightforward symmetry analysis. Our results suggest that nonlinear phononics can be used to control and switch the orientation of induced transient crystal structures.

We thank T. Nova and A. Cavalleri for fruitful discussions. This work was supported by the ETH Zürich and by the ERC Advanced Grant program, No. 291151. Calculations were performed at the Swiss National Supercomputing Centre (CSCS) supported by the Projects No. IDs s624 and No. p504.

*dominik.juraschek@mat.ethz.ch

[1] M. Rini, R. Tobey, N. Dean, J. Itatani, Y. Tomioka, Y. Tokura, R. W. Schoenlein, and A. Cavalleri, Nature (London) **449**, 72 (2007).
[2] R. I. Tobey, D. Prabhakaran, A. T. Boothroyd, and A. Cavalleri, Phys. Rev. Lett. **101**, 197404 (2008).
[3] P. Beaud, S. L. Johnson, E. Vorobeva, U. Staub, R. A. De Souza, C. J. Milne, Q. X. Jia, and G. Ingold, Phys. Rev. Lett. **103**, 155702 (2009).
[4] A. D. Caviglia, R. Scherwitzl, P. Popovich, W. Hu, H. Bromberger, R. Singla, M. Mitrano, M. C. Hoffmann, S. Kaiser, P. Zubko, S. Gariglio, J. M. Triscone, M. Först, and A. Cavalleri, Phys. Rev. Lett. **108**, 136801 (2012).
[5] D. Fausti, R. I. Tobey, N. Dean, S. Kaiser, A. Dienst, M. C. Hoffmann, S. Pyon, T. Takayama, H. Takagi, and A. Cavalleri, Science **331**, 189 (2011).
[6] W. Hu, S. Kaiser, D. Nicoletti, C. R. Hunt, I. Gierz, M. C. Hoffmann, M. Le Tacon, T. Loew, B. Keimer, and A. Cavalleri, Nat. Mater. **13**, 705 (2014).
[7] M. Först, C. Manzoni, S. Kaiser, Y. Tomioka, Y. Tokura, R. Merlin, and A. Cavalleri, Nat. Phys. **7**, 854 (2011).
[8] R. Mankowsky, A. Subedi, M. Först, S. O. Mariager, M. Chollet, H. T. Lemke, J. S. Robinson, J. M. Glownia, M. P. Minitti, A. Frano, M. Fechner, N. A. Spaldin, T. Loew, B. Keimer, A. Georges, and A. Cavalleri, Nature (London) **516**, 71 (2014).
[9] M. Först, R. Mankowsky, H. Bromberger, D. M. Fritz, H. Lemke, D. Zhu, M. Chollet, Y. Tomioka, Y. Tokura, R. Merlin, J. P. Hill, S. L. Johnson, and A. Cavalleri, Solid State Commun. **169**, 24 (2013).
[10] R. Mankowsky, M. Först, T. Loew, J. Porras, B. Keimer, and A. Cavalleri, Phys. Rev. B **91**, 094308 (2015).
[11] M. Fechner and N. A. Spaldin, Phys. Rev. B **94**, 134307 (2016).
[12] Note that this is a nonlinear *phononic* mechanism arising from anharmonic phonon-phonon interactions and not a nonlinear *optical* response to the electric field of the light pulse.
[13] T. F. Nova, A. Cartella, A. Cantaluppi, M. Först, D. Bossini, R. V. Mikhaylovskiy, A. V. Kimel, R. Merlin, and A. Cavalleri, Nat. Phys., doi:10.1038/NPHYS3925 (2016).
[14] D. Treves, J. Appl. Phys. **36**, 1033 (1965).
[15] A. Subedi, A. Cavalleri, and A. Georges, Phys. Rev. B **89**, 220301 (2014).
[16] A. Subedi, Phys. Rev. B **92**, 214303 (2015).
[17] G. Kresse and J. Furthmüller, Comput. Mater. Sci. **6**, 15 (1996).
[18] G. Kresse and J. Furthmüller, Phys. Rev. B **54**, 11169 (1996).
[19] R. L. White, J. Appl. Phys. **40**, 1061 (1969).
[20] A. Togo and I. Tanaka, Scr. Mater. **108**, 1 (2015).
[21] G. I. Csonka, J. P. Perdew, A. Ruzsinszky, P. H. T. Philipsen, S. Lebègue, J. Paier, O. A. Vydrov, and J. G. Ángyán, Phys. Rev. B **79**, 155107 (2009).
[22] G. V. Subba Rao, C. N. R. Rao, and J. R. Ferraro, Appl. Spectrosc. **24**, 436 (1970).
[23] N. Koshizuka and S. Ushioda, Phys. Rev. B **22**, 5394 (1980).
[24] H. Wadati, D. Kobayashi, A. Chikamatsu, R. Hashimoto, M. Takizawa, K. Horiba, H. Kumigashira, T. Mizokawa, A. Fujimori, and M. Oshima, J. Electron Spectrosc. Relat. Phenom. **144–147**, 877 (2005).
[25] M. Eibschütz, Acta Crystallogr. **19**, 337 (1965).
[26] See Supplemental Material at http://link.aps.org/supplemental/10.1103/PhysRevLett.118.054101 for the full lists of calculated phonon eigenfrequencies and anharmonic coefficients and for details on the model pump pulse.